

# Kinematic Analysis and Optimum Design of a Novel $2\text{P}\underline{\text{U}}\text{R}-2\text{R}\underline{\text{P}}\text{U}$ Parallel Robot

TRCIM2019-28-01-01

Yaojun Wang, Bruno Belzile

Jorge Angeles, Qinchuan Li



*Centre for Intelligent Machines, Department of Mechanical Engineering  
McGill University, Montréal, Canada*

## Abstract

A three-dof  $2\underline{P}UR-2\underline{R}PU$  redundantly-actuated parallel-kinematics machine, designed for the machining of complex curved surfaces that requires high-speed and high-precision, is the object of study in this report. The lower-mobility PKM, consisting of two pairs of symmetric, limited-dof limbs, has the advantages of high stiffness, simple kinematic chain, and reduced singularities. The mobility of the robot is investigated via Lie-groups, instead of the well-known Chebyshev-Grübler-Kutzbach formulas, which are not applicable to our case. Then, the inverse-displacement, direct-displacement and corresponding velocity relations are analyzed in detail. Next, by investigating the rank-deficiency of the corresponding Jacobian, three types of singularities, those associated with direct-kinematics, inverse-kinematics and combinations thereof, are analyzed in depth, while constraint singularities are investigated by resorting to constraint wrenches. Moreover, the workspace of both the operation point  $P$  and the tool head, when a tool is added to the moving platform, are derived. It is noteworthy that the local and global dexterity indices are evaluated by resorting to the characteristic length to homogenize the dimensionally inhomogeneous Jacobian matrix at hand, then by gradient optimization to solve the minimum-condition-number problem.

**Keywords:** Parallel-kinematics machine, actuation redundancy, kinematics, Lie-groups, workspace, dexterity

# 1 Introduction

It is known that parallel-kinematics machines (PKMs), comprised of one or multiple kinematic chains, are attracting more and more attention in both academia and industry (Pierrot et al., 2009). A comprehensive enumeration of parallel-kinematics machines and their applications, up to 2006, was provided by Merlet (Merlet, 2006b). A more recent account is available in Chapter 18 of the Springer Handbook of Robotics (Merlet et al., 2016). However, the disadvantages of smaller workspace, limited dexterity and singularity issues are obstacles in the application of PKMs, although they are slowly finding their way into various application environments (Merlet et al., 2016).

In the machining of workpieces with complex curved surfaces, lower-mobility 2R1T<sup>1</sup> PKMs, integrated either with a two-to-three degree-of-freedom (dof) tool head or a two-dof gantry to form five-to-six dof hybrid kinematic machines, have been considerably researched and subsequently applied. The Tricept (Siciliano, 1999), Z3 head (Wahl, 2002), Exechon (Zoppi et al., 2010; Bi and Jin, 2011), and A3 head (Ni et al., 2016) are typical examples of successful applications in the machining industry, which requires high speed and precision. Other applications include medical, such as minimally invasive surgery (Yaşır and Kiper, 2017) and lower-limb rehabilitation (Wang et al., 2018), which have the exact desired motion pattern, namely, roll, pitch, and heave, as the PKM under study.

In response to the applications, many type-synthesis methods of 2R1T PKMs were introduced, such as screw theory (Huang et al., 2017; Xu et al., 2017b), Lie-groups (Li and Hervé, 2014; Fu et al., 2014), and conformal geometric algebra (Song et al., 2018). With the methods at hand, a variety of mechanisms were designed and investigated, such as 3-PRS (Li and Xu, 2007), 3-CUP (Cuan-Urquizo and Rodriguez-Leal, 2013), 3-CRS/PU (Hosseini, 2015), 3-PUU (Wang et al., 2017), Tex3 (Xu et al., 2018a), 2PRU-UPR (Xu et al., 2018b), and 3-CRC (de la Torre and Rodriguez-Leal, 2016), where P, R, S, C, U stand for prismatic, revolute, spherical, cylindrical, and universal joint, respectively.

Compared with the aforementioned 2R1T PKMs without actuation redundancy, their redundantly actuated counterparts offer several advantages (Gosselin and Schreiber, 2018). Indeed, actuation redundancy of overconstrained PKMs can further improve rigidity and precision, while eliminating certain types of singularities. Based on the effect of the redundant active joints on the mobility of a mechanism, PKM redundancy can be basically classified into two types. When the active joints introduce a mobility higher than what is required, the mechanism is said to be kinematically redundant; otherwise, the robot is redundantly actuated (Müller, 2013; Merlet, 1996). Many a study, however, focuses on actuation redundancy, with an ever increased interest on stiffness and on an improved quality of manipulator workspace (Merlet, 1996; Kock and Schumacher, 1998; Gouttefarde and Gosselin, 2005; Wang et al., 2009b,a).

It should be noted that the design of a redundantly actuated lower-mobility PKM with limbs of limited dof<sup>2</sup> is a challenging task (Xu et al., 2017a). Although adding a six-dof limb to a PKM without changing the mobility of the PKM is an easy task, it is difficult to maintain the original mobility after adding a limited-mobility limb. To the best of our knowledge, the types of

---

<sup>1</sup>R: rotation; T: translation

<sup>2</sup>A limb is said to be of limited dof if it is supplied with less than six dof as an open chain.

redundantly actuated reduced-mobility PKMs with limited-dof limbs are currently rare. A brief list was provided by Xu et al. (Xu et al., 2017a). To fill the gap, a redundantly actuated  $2\underline{\text{P}}\text{UR}$ - $2\underline{\text{R}}\text{PU}$   $2\text{R1T}$  PKM is proposed here, where actuated joints appear underlined. When this PKM is used as a machine tool targeting complex curved surfaces, it offers several advantages over their counterparts. First, two of its actuators driving the prismatic joints are mounted on the base, which reduces the movable mass, thereby improving the dynamic response of the mechanical system. Moreover, its architecture is symmetric, with two pairs of identical  $\underline{\text{P}}\text{UR}$  and  $\underline{\text{R}}\text{PU}$  limbs, the former being composed of two cross links with the benefit of eliminating Type-II singularities. Additionally, the chain has a simple kinematic model and a higher stiffness. Last, but not least, the same PKM offers an improved workspace. Despite all the said benefits, redundantly actuated PKMs are subjected to several challenges. The first is the generation of internal forces introduced by redundant actuation, which leads to control requirements that cannot be satisfied with ordinary position-control schemes (Chakarov, 2004). Moreover, motion control and mechanism calibration, among other challenges, should be taken into consideration when designing and applying redundantly actuated PKMs (Lucas et al., 2017).

Performance evaluation is a key issue in the optimum design of PKMs. Most performance indices, such as manipulability and condition number, tell algebraic characteristics of the Jacobian matrix of a PKM, i.e., the dexterity of the robot (Angeles, 2014; Craig, 2005). However, when computing the Jacobian condition number, required to assess the robot dexterity, the disparate units of the matrix in question prevent the computation of its norm. To cope with this problem, a *characteristic length* (Angeles, 2014) is introduced.

The paper is organized as follows: We describe first the  $2\underline{\text{P}}\text{UR}$ - $2\underline{\text{R}}\text{PU}$  PKM and analyze its mobility using Lie algebra in Section 2, followed by the inverse-displacement and direct-displacement analyses in Sections 3. After the velocity analysis in Section 4, four singularity types, namely, direct-kinematics, inverse-kinematics, combined singularity, and constraint singularities, are analyzed in detail in Section 5. Considering the physical constraints imposed by the joints, the reachable workspace is analyzed in Section 6. By resorting to the characteristic length to render the Jacobian dimensionally homogeneous, performance evaluation and dexterity analysis of the robot of interest are discussed at length in Section 7. Finally, some remarks are given, together with the conclusions, in Section 8.

## 2 Description, Notation, and Mobility Analysis

### 2.1 Description and Notation

As shown in Figs. 1–3, the  $2\underline{\text{P}}\text{UR}$ - $2\underline{\text{R}}\text{PU}$  PKM is composed of a base platform (BP), two identical  $\underline{\text{P}}\text{UR}$  and two identical  $\underline{\text{R}}\text{PU}$  limbs, both pairs actuated at the corresponding P joint, and a moving platform (MP). The  $i$ th limb for  $i = 1, 2, 3, 4$ , is  $A_i B_i C_i$ .

As shown in Fig. 1, a Cartesian coordinate frame,  $\mathcal{B}(X, Y, Z)$ , is attached to the fixed base at the intersection  $O$  of the lines  $B_1 B_2$  and  $C_3 C_4$ . A moving coordinate frame,  $\mathcal{P}(U, V, W)$ , is attached to the moving platform at  $P$ , the midpoint of the line segment  $\overline{A_3 A_4}$ . Let the  $X$ - and the  $U$ -axes point in the direction of vectors  $\overrightarrow{B_1 B_2}$  and  $\overrightarrow{A_2 A_1}$ , respectively. Additionally, a limb-coordinate

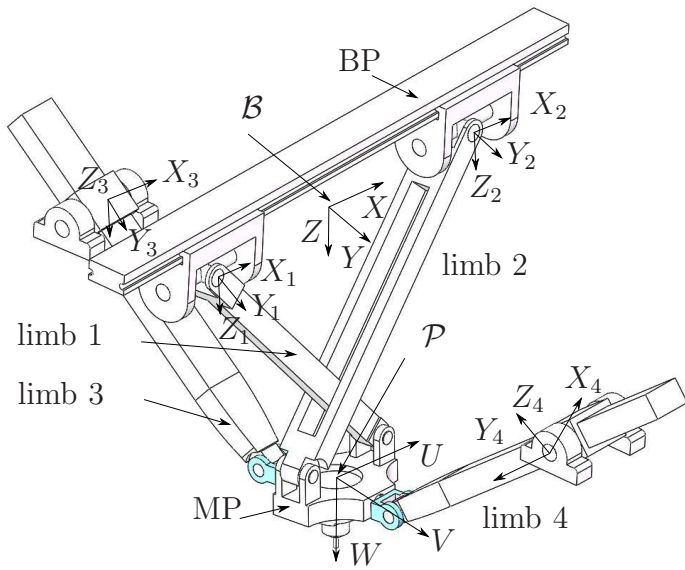


Figure 1: 2PUR-2RPU parallel manipulator

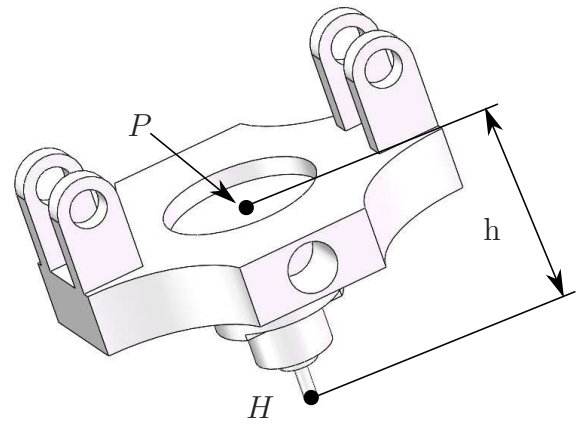
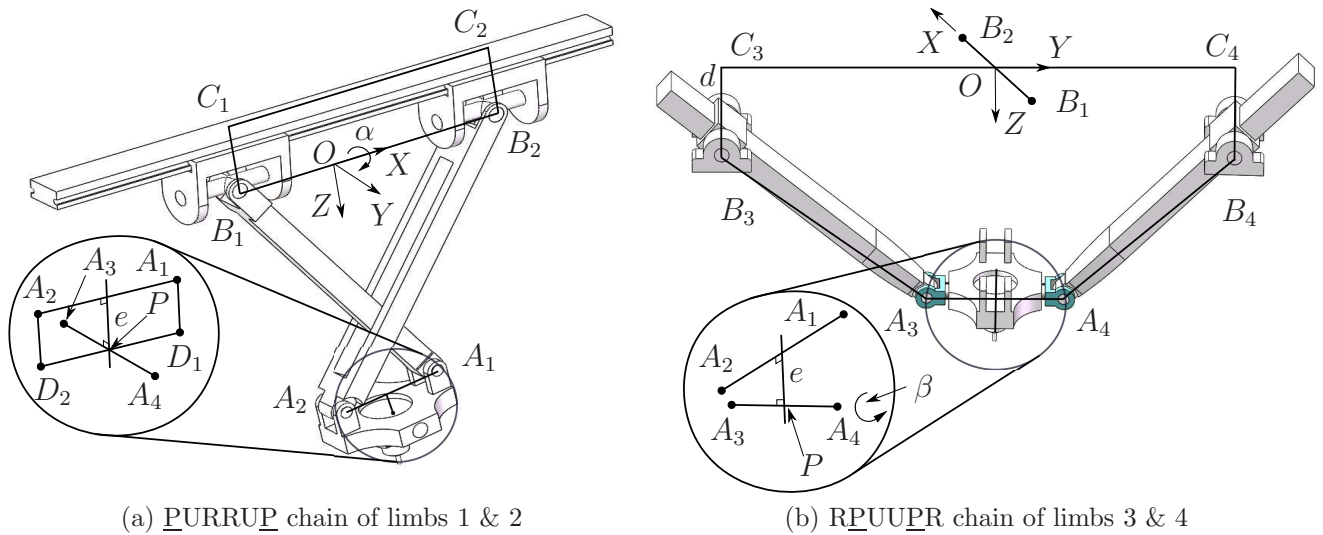


Figure 2: Tool and MP



(a) PURRUP chain of limbs 1 & 2

(b) RPUUPR chain of limbs 3 & 4

Figure 3: Dimensions of the 2PUR-2RPU PKM

frame  $\mathcal{B}_i(X_i, Y_i, Z_i)$ , for  $i = 1, 2, 3, 4$ , is attached to the  $i$ th limb at point  $B_i$ . When  $i = 1, 2$ , the  $X_i, Y_i$ -axes of the limb frames are the revolute axes of the respective U-joints, while the remaining two limb frames define the  $X_i$ -axes as the revolute joints, and the  $Y_i$ -axes in the direction of  $\overrightarrow{B_i A_i}$ , respectively.

Let:  $A_i$ , for  $i = 1, 2$ , denotes a landmark point of each of the two R joints mounted on the MP, as shown in Fig. 3a; for  $i = 3, 4$ ,  $A_i$  denotes the center of each of the two U joints mounted on the MP, as shown in Fig. 3b. As well,  $B_i$ , for  $i = 1, 2$ , denotes the center of each of the two U joints mounted on the BP; for  $i = 3, 4$ ,  $B_i$  denotes a landmark point of each of the two fixed R joints. Line  $B_1 B_2$  is horizontal. Moreover, each  $C_i$ , for  $i = 3, 4$ , is the intersecting point between the vertical line of  $B_i$  and the horizontal plane of line  $B_1 B_2$ . Thus, one can appreciate that  $B_1 B_2 \parallel C_1 C_2$ ,  $B_3 B_4 \parallel C_3 C_4$  and  $B_1 B_2 \perp B_3 B_4$ . Furthermore, each  $D_i$ , for  $i = 1, 2$ , is the projection point of  $A_i$  onto the  $U$ -axis of the frame  $\mathcal{P}$ . It is noteworthy that  $C_1$  and  $C_2$  are not fixed to the base but move with  $B_1$  and  $B_2$ , respectively, along the direction of the corresponding P joint.

## 2.2 Mobility Analysis

### 2.2.1 The Displacement Lie-group and its Subgroups

The motion of the moving platform of the PKM of interest is now investigated by means of Lie algebra (Hervé, 1978). A total of 12 displacement subgroups of the group of rigid-body displacements was first identified by Hervé (Hervé, 1978) and then applied by Angeles (Angeles, 2004) to the qualitative synthesis of parallel manipulators. Four subgroups, of interest to this study, are recalled for quick reference.

1.  $\mathcal{R}(\mathcal{A})$ , the revolute subgroup of rotations about axis  $\mathcal{A}$ .
2.  $\mathcal{P}(\mathbf{e})$ , the prismatic subgroup of translations along the direction of the unit vector  $\mathbf{e}$ .
3.  $\mathcal{F}(\mathbf{w})$ , the planar subgroup of one rotation about an axis parallel to the unit vector  $\mathbf{w}$  and two independent translations in a plane normal to the same vector.
4.  $\mathcal{T}_2(\mathbf{u}, \mathbf{v})$ , the planar-translation subgroup of translations in the directions of the two distinct unit vectors  $\mathbf{u}$  and  $\mathbf{v}$ .

The definition of *kinematic bond* is recalled here: this is a set of displacements stemming from the product of displacement subgroups (Caro et al., 2010), while a bond itself need not be a subgroup. Upon using the Lie subgroups for the mobility analysis of parallel manipulators, Li et al. (Li et al., 2004) applied the Lie subgroups of displacements to limited-mobility parallel manipulators and obtained an exhaustive enumeration of 3R2T five-dof symmetrical parallel manipulators. Here we recall a list of *mechanical generators* of Lie subgroups of interest to the paper.

1. Mechanical generators of  $\mathcal{F}(\mathbf{w})$ 
  - (a)  $\{\mathcal{R}(A, \mathbf{w}) \bullet \mathcal{R}(B, \mathbf{w}) \bullet \mathcal{R}(C, \mathbf{w})\}$
  - (b)  $\{\mathcal{R}(A, \mathbf{w}) \bullet \mathcal{R}(B, \mathbf{w}) \bullet \mathcal{P}(\mathbf{u})\}$ , for  $\mathbf{w} \perp \mathbf{u}$

2. Mechanical generators of  $\mathcal{T}_2(\mathbf{u}, \mathbf{v})$

$$(a) \{ \mathcal{R}(A, \mathbf{w}) \bullet \mathcal{R}(B, \mathbf{w}) \}, \quad \text{for } \mathbf{w} \perp \mathbf{u}, \mathbf{v}$$

### 2.2.2 Mobility Analysis of the 2PUR-2RPU PKM

It is noteworthy that the well-known Chebyshev-Grübler-Kutzbach mobility criterion fails to provide the mobility of the mechanism at hand, which is a *paradoxical chain* in Hervé's classification (Hervé, 1999), thereby excluding the possibility of mobility analysis by this criterion. In the three types of kinematic chains proposed by Hervé, only trivial chains can be analyzed by the above-mentioned criterion (Hervé, 1999), while the mobility of exceptional and paradoxical chains is to be determined by resorting to other methods. A Lie-group analysis is used instead to investigate the mobility of interest. It is noted that screw theory is another powerful tool to this end, very useful when Lie subgroups cannot be applied.

The motion set of the moving platform in a closed-loop chain is the intersection of the kinematic bonds generated by all the limb-kinematic chains connecting the BP to the MP, i.e.,

$$\mathcal{M} = \bigcap_{i=1}^n \{ \mathcal{L}_i \} \quad (1)$$

where  $\mathcal{M}$  is the motion set of the moving platform,  $\mathcal{L}_i$  representing the  $i$ th kinematic bond generated by the  $i$ th-limb chain, and  $n$  the number of limb-chains. Since there are two chains in the manipulator, the PURRUP chain  $\mathcal{L}_1$  and the RPUUPR chain  $\mathcal{L}_2$ , the motion set of the platform can be found as the intersection of the kinematic bonds of these two chains, i.e.,

$$\mathcal{M} = \mathcal{L}_1 \cap \mathcal{L}_2 \quad (2)$$

Similarly, the motion set of each of the two chains can be obtained as the intersection of the two corresponding subchains, i.e.,

$$\mathcal{L}_1 = \mathcal{L}_{11} \cap \mathcal{L}_{12} \quad (3)$$

$$\mathcal{L}_2 = \mathcal{L}_{21} \cap \mathcal{L}_{22} \quad (4)$$

where  $\mathcal{L}_1$  is the closed kinematic chain of Fig. 3a,  $\mathcal{L}_2$  that of Fig. 3b. Moreover,  $\mathcal{L}_{11}$ ,  $\mathcal{L}_{12}$ ,  $\mathcal{L}_{21}$  and  $\mathcal{L}_{22}$  are the four bonds of the subchains of limbs 1,2,3,4, respectively, i.e.,

$$\mathcal{L}_{11} = \mathcal{P}(X) \bullet \mathcal{R}(B_1, X) \bullet \mathcal{R}(B_1, V) \bullet \mathcal{R}(A_1, V) \quad (5)$$

$$\mathcal{L}_{12} = \mathcal{P}(X) \bullet \mathcal{R}(B_2, X) \bullet \mathcal{R}(B_2, V) \bullet \mathcal{R}(A_2, V) \quad (6)$$

$$\mathcal{L}_{21} = \mathcal{R}(B_3, X) \bullet \mathcal{P}(\mathbf{e}_1) \bullet \mathcal{R}(A_3, X) \bullet \mathcal{R}(A_3, V) \quad (7)$$

$$\mathcal{L}_{22} = \mathcal{R}(B_4, X) \bullet \mathcal{P}(\mathbf{e}_2) \bullet \mathcal{R}(A_4, X) \bullet \mathcal{R}(A_4, V) \quad (8)$$

It is recalled that the bond product is *idempotent* (Caro et al., 2010), i.e.,

$$\mathcal{L}(\cdot) \bullet \mathcal{L}(\cdot) = \mathcal{L}(\cdot) \quad (9)$$

Therefore, the motion  $\mathcal{M}_i$  generated by the symmetric chains can be identified as

$$\mathcal{L}_1 = \{\mathcal{F}(V) \bullet \mathcal{R}(B_1, X)\} \cap \{\mathcal{F}(V) \bullet \mathcal{R}(B_2, X)\} = \mathcal{F}(V) \bullet \mathcal{R}(X) \quad (10)$$

$$\mathcal{L}_2 = \{\mathcal{F}(X) \bullet \mathcal{R}(A_3, V)\} \cap \{\mathcal{F}(X) \bullet \mathcal{R}(A_4, V)\} = \mathcal{F}(X) \bullet \mathcal{R}(V) \quad (11)$$

Thus, the motion set of the platform  $\mathcal{M}$  is given as

$$\{\mathcal{M}\} \equiv \{\mathcal{L}_1\} \cap \{\mathcal{L}_2\} = \{\mathcal{F}(V) \bullet \mathcal{R}(X)\} \cap \{\mathcal{F}(X) \bullet \mathcal{R}(V)\} \quad (12)$$

$$= \{\mathcal{R}(V) \bullet \mathcal{P}(U) \bullet \mathcal{P}(W) \bullet \mathcal{R}(X)\} \cap \{\mathcal{R}(X) \bullet \mathcal{P}(Y) \bullet \mathcal{P}(Z) \bullet \mathcal{R}(V)\} \quad (13)$$

$$= \mathcal{P}(\mathbf{p}) \bullet \mathcal{R}(V) \bullet \mathcal{R}(X) \quad (14)$$

This three-degree-of-freedom motion set is not a Lie subgroup, as it lies outside the 12 subgroups in Hervé's classification (Hervé, 1999). The platform is capable of two rotations about corresponding skew axes,  $X$  and  $V$ , at right angles, and one translation along the vector  $\mathbf{p} = \overrightarrow{OP}$ , normal to  $V$ . It is noteworthy that none of the 12 Lie subgroups identified by Hervé (Hervé, 1978) involves two rotation subgroups. We define  $\alpha, \beta$  as the angles of rotation about the  $X$  and the  $V$  axes, respectively,  $\zeta$  as the translation along the direction of  $\mathbf{p}$ .

## 3 Displacement Analysis

### 3.1 Inverse-displacement Analysis

When the independent vector of pose variables  $\mathbf{x} = [\alpha, \beta, \zeta]^T$  of the moving platform is given, the calculation of vector  $\mathbf{q} = [q_1, q_2, q_3, q_4]^T$  of actuated joint variables of  $\overline{OB_1}$ ,  $\overline{OB_2}$ ,  $\overline{B_3A_3}$  and  $\overline{B_4A_4}$ ,



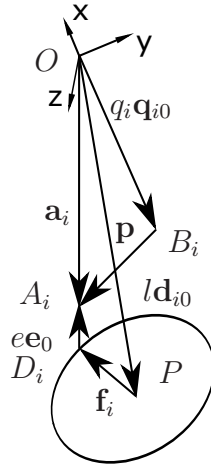


Figure 4: Geometry of one PUR limb

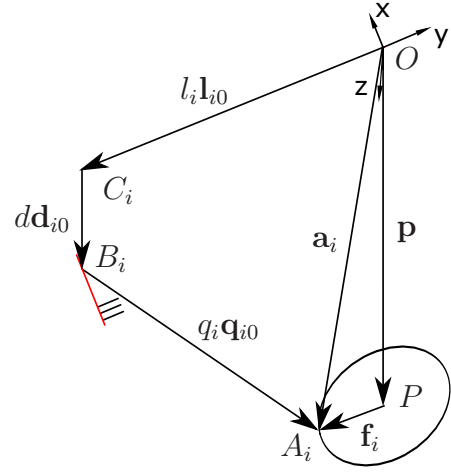


Figure 5: Geometry of one RPU limb

respectively, called the inverse-displacement solution, is straightforward, as is usual in PKMs. As shown in Fig. 4, the vector-loop equation (Merlet, 2006b; Tsai, 1999) for the  $i$ th link, for  $i = 1, 2$ , can be written as

$$\mathbf{p} + \mathbf{f}_i + e\mathbf{e}_0 = q_i \mathbf{q}_{i0} + l \mathbf{d}_{i0} \quad (15)$$

where  $\mathbf{f}_i = \overrightarrow{PD_i}$ , for  $i = 1, 2$ , while  $\mathbf{q}_{i0}$  is the unit vector of the  $i$ th actuator displacement. Furthermore,  $e$  represents the distance between the two lines  $A_1A_2$  and  $A_3A_4$ , while  $\mathbf{e}_0$  is the unit vector in the opposite direction of the  $W$ -axis shown in Fig. 1. Finally,  $l$  represents the length of link  $B_iA_i$ , and  $\mathbf{d}_{i0}$  is a unit vector parallel to  $\overrightarrow{B_iA_i}$ , for  $i = 1, 2$ .

Likewise, referring to Fig. 5, for  $i = 3, 4$ , the vector-loop equation of the RPU link can be obtained as

$$\mathbf{p} + \mathbf{f}_i = l_i \mathbf{l}_{i0} + d \mathbf{d}_{i0} + q_i \mathbf{q}_{i0} \quad (16)$$

where  $\mathbf{f}_i = \overrightarrow{PA_i}$ , for  $i = 3, 4$ , while  $l_i$  represents the magnitude of  $\overrightarrow{OC_i}$ , and  $\mathbf{l}_{i0}$  is the unit vector in the direction of  $\overrightarrow{OC_i}$ , for  $i = 3, 4$ . Moreover,  $\mathbf{d}_{i0}$  is a unit vector parallel to  $\overrightarrow{C_iB_i}$ , and  $d$  the length of  $C_iB_i$ , for  $i = 3, 4$ .

Upon taking the norm of both sides of Eq. (15) and rearranging terms, while considering that  $\mathbf{f}_i \perp \mathbf{e}_0$ , we obtain

$$q_i^2 + 2\mathbf{q}_{i0}^T \mathbf{d}_{i0} l q_i + l^2 - \zeta^2 - f_i^2 - e^2 - 2\mathbf{p}^T \mathbf{f}_i - 2e\mathbf{p}^T \mathbf{e}_0 = 0, \quad i = 1, 2 \quad (17)$$

Hence, the inverse-kinematics solutions are obtained as

$$q_i = -\mathbf{q}_{i0}^T \mathbf{d}_{i0} l \pm \sqrt{(\mathbf{q}_{i0}^T \mathbf{d}_{i0} l)^2 + \zeta^2 + f_i^2 + e^2 - l^2 + 2\mathbf{p}^T \mathbf{f}_i + 2e\mathbf{p}^T \mathbf{e}_0}, \quad i = 1, 2 \quad (18)$$

Similarly, upon taking the norm of both sides of Eq. (16) and rearranging terms, while considering that  $\mathbf{p} \perp \mathbf{f}_i$  for  $i = 3, 4$ , we obtain

$$q_i^2 + 2\mathbf{q}_{i0}^T(l_i\mathbf{l}_{i0} + d\mathbf{d}_{i0})q_i + l_i^2 + d^2 - \zeta^2 - f_i^2 = 0, \quad i = 3, 4 \quad (19)$$

Therefore,

$$q_i = -\mathbf{q}_{i0}^T(l_i\mathbf{l}_{i0} + d\mathbf{d}_{i0}) \pm \sqrt{(\mathbf{q}_{i0}^T(l_i\mathbf{l}_{i0} + d\mathbf{d}_{i0}))^2 + \zeta^2 + f_i^2 - l_i^2 - d^2}, \quad i = 3, 4 \quad (20)$$

thereby obtaining two solutions per actuator. Hence,  $2^4 = 16$  inverse-kinematics solutions for a given platform pose are possible.

We investigate next the solution of the inverse-displacement problem. Let the position vector of point  $A_i$ , for  $i = 1, 2, 3, 4$ , expressed in frames  $\mathcal{B}$  and  $\mathcal{P}$ , be denoted by  $[\mathbf{a}_i]_{\mathcal{B}}$  and  $[\mathbf{a}_i]_{\mathcal{P}}$ , respectively. Furthermore, the rotation matrix from  $\mathcal{P}$  to  $\mathcal{B}$  is represented by  $[\mathbf{Q}]_{\mathcal{B}}$ , the subscript of the brackets identifying the coordinate frame in which a vector or a matrix is expressed. For brevity, the subscript will be omitted whenever the coordinate frame is the fixed frame  $\mathcal{B}$ . The matrix rotating frame  $\mathcal{B}$  to frame  $\mathcal{P}$  is calculated below:

$$\mathbf{Q} = \mathbf{Q}_x(\alpha)\mathbf{Q}_y(\beta) = \begin{bmatrix} 1 & 0 & 0 \\ 0 & \cos \alpha & -\sin \alpha \\ 0 & \sin \alpha & \cos \alpha \end{bmatrix} \begin{bmatrix} \cos \beta & 0 & \sin \beta \\ 0 & 1 & 0 \\ -\sin \beta & 0 & \cos \beta \end{bmatrix} \quad (21)$$

$$= \begin{bmatrix} \cos \beta & 0 & \sin \beta \\ \sin \alpha \sin \beta & \cos \alpha & -\sin \alpha \cos \beta \\ -\cos \alpha \sin \beta & \sin \alpha & \cos \alpha \cos \beta \end{bmatrix} \quad (22)$$

Moreover, we have

$$\mathbf{a}_i = \mathbf{Q}_{\mathcal{P}}[\mathbf{a}_i]_{\mathcal{P}} + \mathbf{p}, \quad \text{for } i = 1, 2, 3, 4 \quad (23)$$

and

$$[\mathbf{a}_1]_{\mathcal{P}} = [f_1 \quad 0 \quad -e]^T, \quad [\mathbf{a}_2]_{\mathcal{P}} = [-f_1 \quad 0 \quad -e]^T \quad (24a)$$

$$[\mathbf{a}_3]_{\mathcal{P}} = [0 \quad -f_3 \quad 0]^T, \quad [\mathbf{a}_4]_{\mathcal{P}} = [0 \quad f_3 \quad 0]^T \quad (24b)$$

where  $f_i$  is the magnitude of  $\mathbf{f}_i$ ; and  $\mathbf{p} = [0 \quad -\zeta \sin \alpha \quad \zeta \cos \alpha]^T$  denotes the position vector of point  $P$ . Let  $\theta_i$  denote the angle between  $Z_i$  and  $\overrightarrow{B_i A_i}$  for  $i = 1, 2$ , and between  $Y_i$  and  $Y$  for  $i = 3, 4$ . Moreover,  $\mathbf{a}_i$  can be obtained through another rotation matrix  $\mathbf{Q}_i$  that represents the rotation from frame  $\mathcal{B}$  to frame  $\mathcal{B}_i$ , thus obtaining

$$\mathbf{a}_i = \mathbf{Q}_i[\mathbf{a}_i]_{\mathcal{B}_i} + \mathbf{b}_i, \quad \text{for } i = 1, 2, 3, 4 \quad (25)$$

with

$$\mathbf{Q}_1 = \mathbf{Q}_2 = \mathbf{Q}_x(\alpha) = \begin{bmatrix} 1 & 0 & 0 \\ 0 & \cos \alpha & -\sin \alpha \\ 0 & \sin \alpha & \cos \alpha \end{bmatrix} \quad (26a)$$

$$\mathbf{Q}_3 = \mathbf{Q}_x(\theta_3) = \begin{bmatrix} 1 & 0 & 0 \\ 0 & \cos \theta_3 & -\sin \theta_3 \\ 0 & \sin \theta_3 & \cos \theta_3 \end{bmatrix} \quad (26b)$$

$$\mathbf{Q}_4 = \mathbf{Q}_x(\theta_4) = \begin{bmatrix} 1 & 0 & 0 \\ 0 & \cos \theta_4 & -\sin \theta_4 \\ 0 & \sin \theta_4 & \cos \theta_4 \end{bmatrix} \quad (26c)$$

where the origin  $B_i$  of the respective limb frame, expressed in  $\mathcal{B}$ , is obtained as

$$\mathbf{b}_1 = [q_1 \ 0 \ 0]^T, \mathbf{b}_2 = [q_2 \ 0 \ 0]^T, \mathbf{b}_3 = [0 \ -l_3 \ d]^T, \mathbf{b}_4 = [0 \ l_3 \ d]^T \quad (27)$$

and the position vector of point  $A_i$ ,  $[\mathbf{a}_i]_{\mathcal{B}_i}$ , expressed in  $\mathcal{B}_i$ , for  $i = 1, 2, 3, 4$ , is given by

$$[\mathbf{a}_1]_{\mathcal{B}_1} = [l \sin \theta_1 \ 0 \ l \cos \theta_1]^T, [\mathbf{a}_2]_{\mathcal{B}_2} = [-l \sin \theta_2 \ 0 \ l \cos \theta_2]^T \quad (28a)$$

$$[\mathbf{a}_3]_{\mathcal{B}_3} = [0 \ q_3 \ 0]^T, [\mathbf{a}_4]_{\mathcal{B}_4} = [0 \ q_4 \ 0]^T \quad (28b)$$

Upon recalling Eqs. (23) and (25), and denoting the same position vectors of points  $A_i$  in the frame  $\mathcal{B}$  through different paths, we substitute the right-hand sides of these two equations with their corresponding entries, thus obtaining

$$l \sin \theta_1 + q_1 = f_1 \cos \beta - e \sin \beta \quad (29a)$$

$$l \cos \theta_1 = \zeta - f_1 \sin \beta - e \cos \beta \quad (29b)$$

$$q_2 - l \sin \theta_2 = -f_1 \cos \beta - e \sin \beta \quad (29c)$$

$$l \cos \theta_2 = \zeta + f_1 \sin \beta - e \cos \beta \quad (29d)$$

$$q_3 \cos \theta_3 - l_3 = -f_3 \cos \alpha - \zeta \sin \alpha \quad (29e)$$

$$q_3 \sin \theta_3 + d = -f_3 \sin \alpha + \zeta \cos \alpha \quad (29f)$$

$$q_4 \cos \theta_4 + l_3 = f_3 \cos \alpha - \zeta \sin \alpha \quad (29g)$$

$$q_4 \sin \theta_4 + d = f_3 \sin \alpha + \zeta \cos \alpha \quad (29h)$$

Now let

$$g_{11} = l \sin \theta_1, \quad g_{12} = l \cos \theta_1 \quad (30a)$$

$$g_{21} = l \sin \theta_2, \quad g_{22} = l \cos \theta_2 \quad (30b)$$

$$g_{31} = q_3 \sin \theta_3, \quad g_{32} = q_3 \cos \theta_3 \quad (30c)$$

$$g_{41} = q_4 \sin \theta_4, \quad g_{42} = q_4 \cos \theta_4 \quad (30d)$$

Upon substitution of expressions (30a) through (30d) into Eqs. (29a) through (29h),  $g_{ij}$  can be obtained as

$$g_{11} = \sqrt{l^2 - (\zeta - f_1 \sin \beta - e \cos \beta)^2}, \quad g_{12} = \zeta - f_1 \sin \beta - e \cos \beta \quad (31a)$$

$$g_{21} = \sqrt{l^2 - (\zeta + f_1 \sin \beta - e \cos \beta)^2}, \quad g_{22} = \zeta + f_1 \sin \beta - e \cos \beta \quad (31b)$$

$$g_{31} = \zeta \cos \alpha - f_3 \sin \alpha - d, \quad g_{32} = l_3 - f_3 \cos \alpha - \zeta \sin \alpha \quad (31c)$$

$$g_{41} = \zeta \cos \alpha + f_3 \sin \alpha - d, \quad g_{42} = -l_3 + f_3 \cos \alpha - \zeta \sin \alpha \quad (31d)$$

Hence, the unique inverse-displacement solution for the 2PUR-2PUR PKM is obtained as

$$\mathbf{q} = \begin{bmatrix} -g_{11} + f_1 \cos \beta - e \sin \beta \\ g_{21} - f_1 \cos \beta - e \sin \beta \\ \sqrt{g_{31}^2 + g_{32}^2} \\ \sqrt{g_{41}^2 + g_{42}^2} \end{bmatrix} \quad (32)$$

### 3.2 Direct-displacement Analysis

First, Eq. (32) leads to

$$g_{11} = f_1 \cos \beta - e \sin \beta - q_1, \quad g_{21} = f_1 \cos \beta + e \sin \beta + q_2 \quad (33a)$$

$$q_3 = \sqrt{g_{31}^2 + g_{32}^2}, \quad q_4 = \sqrt{g_{41}^2 + g_{42}^2} \quad (33b)$$

Substituting  $g_{ij}$  from Eqs. (31a) to (31d) into Eq. (33), then squaring both sides of these equations yields

$$\zeta^2 + 2(q_1 e - f_1 \zeta) \sin \beta - 2(f_1 q_1 + \zeta e) \cos \beta + e^2 + f_1^2 + q_1^2 - l^2 = 0 \quad (34a)$$

$$\zeta^2 + 2(q_2 e + f_1 \zeta) \sin \beta + 2(f_1 q_2 - \zeta e) \cos \beta - e^2 + f_1^2 + q_2^2 - l^2 = 0 \quad (34b)$$

$$\zeta^2 - 2(l_3 f_3 + \zeta d) \cos \alpha + 2(df_3 - l_3 \zeta) \sin \alpha + d^2 + l_3^2 + f_3^2 - q_3^2 = 0 \quad (34c)$$

$$\zeta^2 - 2(l_3 f_3 + \zeta d) \cos \alpha - 2(df_3 - l_3 \zeta) \sin \alpha + d^2 + l_3^2 + f_3^2 - q_4^2 = 0 \quad (34d)$$

Upon adding sidewise Eqs. (34a) and (34b), then subtracting the former from the latter, next proceeding likewise with Eqs. (34c) and (34d), we obtain

$$\zeta^2 + 2e\zeta \cos \beta + \lambda_1 \cos \beta + \lambda_3 \sin \beta + \lambda_5 = 0 \quad (35a)$$

$$2f_1 \zeta \sin \beta + \lambda_2 \cos \beta + \lambda_4 \sin \beta + \lambda_6 = 0 \quad (35b)$$

$$\zeta^2 - 2\mu_2 \cos \alpha - 2d\zeta \cos \alpha + \mu_3 = 0 \quad (35c)$$

$$(\mu_1 - l_3 \zeta) \sin \alpha + \mu_4 = 0 \quad (35d)$$

where

$$\lambda_1 = f_1(q_2 - q_1), \quad \lambda_2 = f_1(q_2 + q_1), \quad \lambda_3 = e(q_2 + q_1) \quad (36a)$$

$$\lambda_4 = e(q_2 - q_1), \quad \lambda_5 = \frac{q_1^2 + q_2^2}{2} + f_1^2 - l^2, \quad \lambda_6 = \frac{q_2^2 - q_1^2}{2} - e^2 \quad (36b)$$

$$\mu_1 = df_3, \quad \mu_2 = l_3 f_3 \quad (36c)$$

$$\mu_3 = -\frac{q_3^2 + q_4^2}{2} + f_3^2 + d^2 + l_3^2 \quad \mu_4 = \frac{q_4^2 - q_3^2}{4} \quad (36d)$$

Equations (35c & 35d) yield

$$\cos \alpha = \frac{\zeta^2 + \mu_3}{2(\mu_2 + d\zeta)}, \quad \sin \alpha = \frac{\mu_4}{l_3\zeta - \mu_1} \quad (37)$$

Upon squaring both sides of Eq. (37), then adding them sidewise yields

$$\frac{(\zeta^2 + \mu_3)^2}{4(\mu_2 + d\zeta)^2} + \frac{\mu_4^2}{(l_3\zeta - \mu_1)^2} = 1 \quad (38)$$

From the foregoing equation we obtain a sixth-degree polynomial in  $\zeta$ :

$$\nu_0\zeta^6 + \nu_1\zeta^5 + \nu_2\zeta^4 + \nu_3\zeta^3 + \nu_4\zeta^2 + \nu_5\zeta + \nu_6 = 0 \quad (39)$$

where  $\nu_i$ ,  $i = 0, 1, \dots, 6$ , is a function of the geometric parameters of the mechanism and its joint coordinates. Once  $\zeta$  is known, Eq. (37) yields one single value for  $\alpha$ , while Eqs. (35a) and (35b) yield one single value for  $\beta$ . It can be concluded that the direct-kinematics of the moving platform admits six MP poses, some feasible, some unfeasible, depending on the nature of the roots of Eq. (39), some real, some complex. However, it is cumbersome to derive all possible configurations of the moving platform through this approach. Hence, for the purpose of control, a numerical method is recommended to solve the direct-displacement problem.

## 4 Velocity Analysis

### 4.1 Vector Loop-Equation

Differentiation of both sides of Eq. (15) with respect to time yields

$$\mathbf{v}_P + \boldsymbol{\omega}_P \times \mathbf{f}_i + e\boldsymbol{\omega}_P \times \mathbf{e}_0 = \dot{q}_i \mathbf{q}_{i0} + l\boldsymbol{\omega}_i \times \mathbf{d}_{i0} \quad \text{for } i = 1, 2 \quad (40)$$

Upon dot-multiplying both sides of Eq. (40) by  $\mathbf{d}_{i0}$  to eliminate the passive variable  $\boldsymbol{\omega}_i$ , we obtain

$$\mathbf{v}_P^T \mathbf{d}_{i0} + (\boldsymbol{\omega}_P \times \mathbf{f}_i)^T \mathbf{d}_{i0} + e(\boldsymbol{\omega}_P \times \mathbf{e}_0)^T \mathbf{d}_{i0} = \dot{q}_i \mathbf{q}_{i0}^T \mathbf{d}_{i0} \quad (41)$$

which, after rearranging, becomes

$$\mathbf{d}_{i0}^T \mathbf{v}_P + (\mathbf{f}_i \times \mathbf{d}_{i0})^T \boldsymbol{\omega}_P + (e \mathbf{e}_0 \times \mathbf{d}_{i0})^T \boldsymbol{\omega}_P = \dot{q}_i \mathbf{d}_{i0}^T \mathbf{q}_{i0} \quad (42)$$

Similarly, differentiation of both sides of Eq. (16) with respect to time yields

$$\mathbf{v}_P + \boldsymbol{\omega}_P \times \mathbf{f}_i = q_i \boldsymbol{\omega}_i \times \mathbf{q}_{i0} + \dot{q}_i \mathbf{q}_{i0} \quad \text{for } i = 3, 4 \quad (43)$$

Then, upon dot-multiplying both sides of Eq. (43) by  $\mathbf{q}_{i0}$ , we obtain

$$\mathbf{v}_P^T \mathbf{q}_{i0} + (\boldsymbol{\omega}_P \times \mathbf{f}_i)^T \mathbf{q}_{i0} = \dot{q}_i \quad (44)$$

which, likewise, upon rearranging, becomes

$$\mathbf{q}_{i0}^T \mathbf{v}_P + (\mathbf{f}_i \times \mathbf{q}_{i0})^T \boldsymbol{\omega}_P = \dot{q}_i \quad (45)$$

Now,  $\mathbf{t}_P = [\mathbf{v}_P^T \quad \boldsymbol{\omega}_P^T]^T$  denotes the twist of the moving platform, while keeping in mind that only three of its six components are independent. We obtain, after straightforward manipulations,

$$\mathbf{K}_p \mathbf{t}_P = \mathbf{J}_q \dot{\mathbf{q}} \quad (46)$$

where

$$\mathbf{J}_q = \begin{bmatrix} \mathbf{d}_{10}^T \mathbf{q}_{10} & 0 & 0 & 0 \\ 0 & \mathbf{d}_{20}^T \mathbf{q}_{20} & 0 & 0 \\ 0 & 0 & 1 & 0 \\ 0 & 0 & 0 & 1 \end{bmatrix}, \quad \mathbf{K}_p = \begin{bmatrix} \mathbf{d}_{10}^T & (\mathbf{f}_1 \times \mathbf{d}_{10})^T + e(\mathbf{e}_0 \times \mathbf{d}_{10})^T \\ \mathbf{d}_{20}^T & (\mathbf{f}_2 \times \mathbf{d}_{20})^T + e(\mathbf{e}_0 \times \mathbf{d}_{20})^T \\ \mathbf{q}_{30}^T & (\mathbf{f}_3 \times \mathbf{q}_{30})^T \\ \mathbf{q}_{40}^T & (\mathbf{f}_4 \times \mathbf{q}_{40})^T \end{bmatrix} \quad (47)$$

## 4.2 Velocity Equation

Differentiation of both sides of Eq. (32) with respect to time yields

$$\mathbf{J}_r \dot{\mathbf{q}} = \mathbf{K} \mathbf{t} \quad (48)$$

where  $\mathbf{t} \equiv [\dot{\alpha} \ \dot{\beta} \ \dot{\zeta}]^T$  denotes the three-dimensional twist of the MP, composed of the two independent angular speeds  $\dot{\alpha}$  and  $\dot{\beta}$ , along with the speed  $\dot{\zeta}$ . Furthermore,

$$\mathbf{J}_r = \begin{bmatrix} J_{11} & 0 & 0 & 0 \\ 0 & J_{22} & 0 & 0 \\ 0 & 0 & J_{33} & 0 \\ 0 & 0 & 0 & J_{44} \end{bmatrix}, \quad \mathbf{K} = \begin{bmatrix} 0 & K_{11} & K_{13} \\ 0 & K_{21} & K_{23} \\ K_{32} & 0 & K_{33} \\ K_{42} & 0 & K_{43} \end{bmatrix} \quad (49)$$

with

$$\begin{aligned} J_{11} &= g_{11}, & J_{22} &= g_{21}, & J_{33} &= \sqrt{g_{31}^2 + g_{32}^2}, & J_{44} &= \sqrt{g_{41}^2 + g_{42}^2} \\ K_{11} &= -g_{11}f_1 \sin \beta - g_{11}e \cos \beta + (\zeta - f_1 \sin \beta - e \cos \beta)(e \sin \beta - f_1 \cos \beta) \\ K_{21} &= g_{21}f_1 \sin \beta - g_{21}e \cos \beta - (\zeta + f_1 \sin \beta - e \cos \beta)(f_1 \cos \beta + e \sin \beta) \\ K_{13} &= \zeta - f_1 \sin \beta - e \cos \beta, & K_{23} &= -f_1 \sin \beta - \zeta + e \cos \beta \\ K_{32} &= -g_{31}(\zeta \sin \alpha + f_3 \cos \alpha) + g_{32}(f_3 \sin \alpha - \zeta \cos \alpha) \\ K_{33} &= g_{31} \cos \alpha - g_{32} \sin \alpha \\ K_{42} &= g_{41}(-\zeta \sin \alpha + f_3 \cos \alpha) - g_{42}(f_3 \sin \alpha + \zeta \cos \alpha) \\ K_{43} &= g_{41} \cos \alpha - g_{42} \sin \alpha \end{aligned}$$

## 5 Singularity Analysis

When any of the two Jacobian matrices becomes either singular or rank-deficient, as the case may be, the mechanism finds itself at a singularity, as explained below. At a singular configuration, the system loses either stiffness or mobility, thereby falling into either uncontrollable motion or deficient performance. From a result on the singularity analysis of PKMs (Gosselin and Angeles, 1990), the singularity problem of general closed-loop kinematic chains, such as PKMs, can be divided into three types: Type-I, direct-kinematics singularity; Type-II, inverse-kinematics singularity; and Type-III, combined singularity. Besides the aforementioned singularities, there may exist other types in constrained PKMs, namely, *constraint-singularities* (Zlatanov et al., 2002), which cannot be identified by the rank-deficiency of the Jacobian matrices. At such singularities, the constraint wrenches degenerate, thereby increasing instantaneously the degree of freedom of the MP. Thus, it is essential to look for constraint singularities before eliminating the passive velocities.

Recalling Eq. (46) and considering the rank deficiency of the matrices concerned, the three types of singularity are now identified, while constraint-singularity is analyzed by resorting to constraint wrenches.

## 5.1 Type-I: Direct-kinematics Singularity

A singularity of this type occurs when the  $4 \times 6$   $\mathbf{K}_p$  matrix is rank-deficient. In order to characterize the rank-deficiency of interest, let

$$\mathbf{n}_i = \begin{cases} (\mathbf{f}_i + e\mathbf{e}_0) \times \mathbf{d}_{i0}, & \text{if } i = 1, 2 \\ \mathbf{f}_i \times \mathbf{q}_{i0}, & \text{if } i = 3, 4 \end{cases} \quad (51)$$

Vector  $\mathbf{n}_i$  is normal to the plane defined by points  $P$ ,  $A_i$ , and  $B_i$ . One can readily notice that  $\mathbf{n}_1$  and  $\mathbf{n}_2$  are parallel, while  $\mathbf{n}_3$  is parallel to  $\mathbf{n}_4$ . However, the foregoing linear-dependency does not lead to the rank-deficiency of  $\mathbf{K}_p$ . If two or more of the vectors of  $\mathbf{K}_p$  vanish, then the matrix is rank-deficient. Indeed, let us assume that

$$\mathbf{n}_i = \mathbf{0}, \quad \text{for } i \in \{1, 2\} \quad \text{and} \quad \mathbf{n}_j = \mathbf{0}, \quad \text{for } j \in \{3, 4\} \quad (52)$$

which means that (i) line  $A_iB_i$  coincides with line  $PA_i$ , for the  $\underline{\text{PURRUP}}$  chain, when  $i = 1, 2$  and (ii)  $A_iB_i$  coincides with the  $V$ -axis of the moving frame  $\mathcal{P}$ , for the  $\underline{\text{RPUUPR}}$  chain, when  $i = 3, 4$ . It is noteworthy, however, that only the condition for  $i = 3, 4$  is possible, as  $A_1B_1$  and  $A_2B_2$  cannot coincide with lines  $PA_1$  and  $PA_2$ , respectively, because of interference. As a result, the mechanism acquires one or more degrees of freedom in the presence of this singularity, even when all the actuators are locked.

## 5.2 Type-II: Inverse-kinematics Singularity

On the other hand, the mechanism finds itself at an inverse-kinematics singular posture when  $\mathbf{J}_q$  is singular. The determinant of the diagonal matrix  $\mathbf{J}_q$  of Eq. (47) vanishes if at least one of its first two diagonal entries does, i.e., if

$$\mathbf{d}_{i0}^T \mathbf{q}_{i0} = 0, \quad \text{for } i \in \{1, 2\} \quad (53)$$

Under the above singularity,  $OB_i \perp B_iA_i$ . The perpendicularity of these two lines leads to a posture under which the axis of at least one of the legs is perpendicular to its actuator direction, the mechanism thus losing one or two degrees of freedom instantaneously, depending on the number of perpendicularity cases. This type of singularity, however, will not occur in the mechanism at hand because of the geometric constraints imposed by the link shapes of the two cross links,  $B_1A_1$  and  $B_2A_2$ , by design.

## 5.3 Type-III: Combined Singularity

The combined singularity occurs when both  $\mathbf{K}_p$  and  $\mathbf{J}_q$  are rank-deficient simultaneously. Since the second singularity is precluded by the geometry of the robot, this third type of singularity is also precluded.



## 5.4 Constraint-Singularity

From the viewpoint of constraints, a kinematic chain with reduced mobility experiences internal constraint wrenches. The two limb chains, of four-dof, exert one constraint on the three-dof MP. We define  $\mathbf{p}_\perp$  as a unit vector that is perpendicular to  $\mathbf{p}$  in the plane spanned by lines  $A_1B_1$  and  $A_2B_2$ . When  $\mathbf{p}_\perp$  is parallel to  $V$ , this constraint vanishes, and the MP, as a result, finds itself at a posture of four dof instantaneously. Thus, Eq. (12) has the form:

$$\{\mathcal{M}\} \equiv \{\mathcal{L}_1\} \cap \{\mathcal{L}_2\} = \{\mathcal{F}(V) \bullet \mathcal{R}(X)\} \cap \{\mathcal{F}(X) \bullet \mathcal{R}(V)\} \quad (54)$$

$$= \{\mathcal{R}(V) \bullet \mathcal{P}(\mathbf{p}) \bullet \mathcal{P}(\mathbf{p}_\perp) \bullet \mathcal{R}(X)\} \cap \{\mathcal{R}(X) \bullet \mathcal{P}(\mathbf{p}) \bullet \mathcal{P}(V) \bullet \mathcal{R}(V)\} \quad (55)$$

$$= \mathcal{F}(V) \bullet \mathcal{R}(X) \quad (56)$$

This means that the two-limb chains have the same constraints on the MP. Under these constraints, the MP can undergo two independent translations and two independent rotations. This type of singularities, however, will never occur in the robot because of the geometric constraints imposed, ensuring that  $\mathbf{p}_\perp$  cannot be parallel to  $V$ .

## 6 Workspace Analysis

### 6.1 Physical Constraints and Algorithms

The reachable workspace of a PKM is defined as the set of points that can be reached by the operation point in the moving platform, and the set of orientations attained by the MP (Merlet, 2006b). The concept is essential to determining the workspace boundaries, its singularities and voids, for the design and performance analysis of a manipulator (Choi et al., 2008). Compared with their serial counterparts, PKMs have relatively small workspaces. Therefore, the workspace of PKMs is an important concept that reflects their performance.

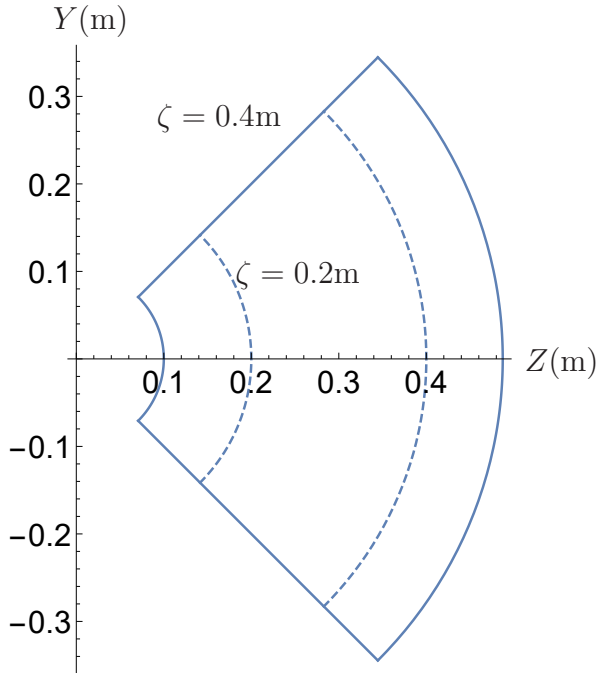
Point  $P$ , located at the center of the moving platform, is the reference point and can only move in the plane spanned by lines  $A_3B_3$  and  $A_4B_4$ . An axially symmetric tool, with its axis passing through  $P$ , as shown in Fig. 2, is to be added, as the need arises. Hence, the workspace problem of the robot can be significantly simplified by investigating the workspace of  $P$  first. We can arbitrarily set  $\beta$  to be 0 because it does not affect the computation of the robot workspace with respect to the reference point  $P$ . By varying the remaining coordinates,  $\alpha$  and  $\zeta$ , one can readily prove that the workspace “volume”<sup>3</sup>  $V$  is given by

$$V = \int_{\zeta_{\min}}^{\zeta_{\max}} \zeta \Delta \alpha d\zeta \quad (57)$$

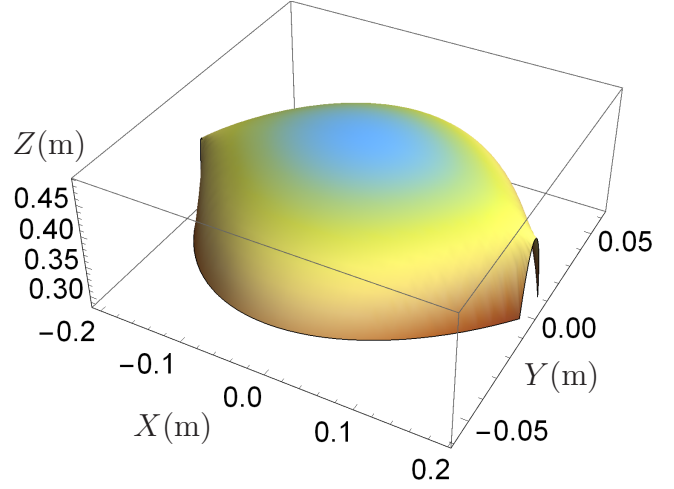
which, in this case, lies in a plane;  $V$  is the area reachable by the said point  $P$ . Considering the architecture constraints of the manipulator,  $\zeta_{\max}$  and  $\zeta_{\min}$  denote the maximum and the minimum

---

<sup>3</sup>Quotation marks intended to acknowledge that, rather than a three-dimensional volume, what we have is a two-dimensional region.



(a) workspace of the reference point  $P$



(b) subdomain of workspace of the tool head  $H$  in case of  $\zeta = 0.2$  m

Figure 6: Reachable workspace of a  $2\underline{P}UR-2\underline{R}PU$  PKM

distance between  $P$  and  $O$ ,  $\Delta\alpha$  being the range of orientation of  $\alpha$ . We assume that the motion range of each prismatic actuator is within  $\pm 0.2$  m, and its rotational range of motion is set as  $\pm\pi/4$ .

## 6.2 Case Studies

The architectural parameters of the manipulator are selected as  $l = 0.6$  m,  $l_3 = 0.4$  m,  $f_i = 0.3$  m (for  $i = 1, 3$ ),  $d = 0.1$  m and  $e = 0$  m. Upon considering the physical constraints of the joints, we let  $\zeta_{min} = 0.1$  m. Next we calculate the range of  $\zeta$  to obtain the reachable workspace of the manipulator. One can readily show that the position of the largest  $\zeta$  is reached when the two U-joints of the  $\underline{P}URR\underline{U}P$  chain find themselves closest to the origin  $O$ . The two U-joints, however, cannot reach the said origin because of the physical constraints imposed by themselves. We assume a limit  $q_{min} = 0.05$  m for  $q_3$  and  $q_4$ . Therefore,

$$\zeta_{max} = \sqrt{l^2 - \left(\frac{f_3 + f_4 + 2q_{min}}{2}\right)^2} \approx 0.4873 \text{ m} \quad (58)$$

Upon recalling Eq. (57) one can readily find  $V = 0.1787$  m<sup>2</sup>. Furthermore, since a tool is added at the point  $P$  in machining applications, the workspace of the tool head is three-dimensional, as

depicted in Fig. 6b, where the optimum length of the tool is 0.2874 m, as derived from condition-number minimization in Subsection 7.2. It is pointed out that, although the workspace of the tool head lies in three-dimensional space, its dof is two rotations plus one translation, obtained by fixing the length of the translational displacement  $\zeta$ , then rotating the MP around two axes  $X$  and  $V$  with feasible  $\alpha$  and  $\beta$ . With varied length of  $\zeta$ , the reachable workspace of the tool head is obtained by the aforementioned geometrical approach.

## 7 Dexterity Analysis

### 7.1 Dexterity Indices

It is of the utmost importance to establish and quantify the different performance characteristics of a mechanism. As most kinematic performance measures are based on the Jacobian, and its invariants, such as determinant, eigenvalues, singular values, and condition number, it is an indispensable matrix in understanding the motion of the end-effector (Patel and Sobh, 2015). Performance indices such as manipulability, defined as the square root of the determinant of  $\mathbf{J}\mathbf{J}^T$  (Yoshikawa, 1985), and the condition number of the Jacobian matrix (Salisbury and Craig, 1982) are well known. The Jacobian  $\mathbf{J}$  of interest is defined as:

$$\mathbf{J} = \mathbf{J}_r^{-1}\mathbf{K} \quad (59)$$

The foregoing  $4 \times 3$  Jacobian  $\mathbf{J}$  is the result of actuation-redundancy, namely, the use of four actuators to control three independent pose variables.

Since, in general, a Jacobian matrix is configuration-dependent, the above-mentioned metrics are local performance indices that give an indication of how far the manipulator posture is from a singularity. It is noteworthy that, in fact, the determinant of a square matrix tells only if and when a matrix is invertible, but it does not tell the *invertibility* of the matrix (Angeles, 2014). The maximum-singular-value based sensitivity indices (Han et al., 2002) suffer from a significant limitations, as they are scale-dependent. Hence, we investigate the numerical properties of the Jacobian matrix using the condition number, rather than the manipulability and the sensitivity.

A posture-independent index, termed the *kinetostatic conditioning index* (KCI), introduced elsewhere (Angeles, 2014), is given by

$$\text{KCI} = \frac{1}{\kappa_{\min}} \times 100\% \quad (60)$$

Since the condition number is bounded from below, the KCI is bounded from above by a value of 100%. Manipulators with a KCI of 100%, those with a minimum condition number of 1.0, are termed *isotropic*, which is one of the objectives of design optimization.

In general, any Jacobian matrix includes both dimensionless entries and entries with units of length, which prevents the computation of the condition number (Merlet, 2006a). To cope with this challenge, a dimensionally homogeneous Jacobian,  $\mathbf{J}_h$ , was proposed (Angeles, 2014) by

means of the concept of *characteristic length*. A performance index, termed the *global conditioning index* (GCI), was introduced to represent the dexterity over the entire workspace, rather than at a certain posture (Gosselin and Angeles, 1991). The GCI is defined as

$$\text{GCI} = \frac{\int_{\mathcal{W}} (1/\kappa) dV}{V} \quad (61)$$

where  $V$  is the volume of the workspace,  $\mathcal{W}$  is the entire robot workspace and  $\kappa$  is the condition number at a particular point of  $\mathcal{W}$ .

It is pointed out, however, that several other approaches are available to cope with the limitations of scale dependence and inhomogeneity, inherent in the Jacobian based metrics. A formulation for the kinematic equations, using the velocity of some points of the end-effector, rather than only one point in it, thus leading to homogeneous Cartesian rates, was proposed by Gosselin (Gosselin, 1992). However, this formulation requires that all joints be of the same type. Thus, kinematic-sensitivity indices for dimensionally inhomogeneous Jacobian matrices, namely, the *maximum rotation sensitivity* and the *maximum point-displacement sensitivity*, were introduced as two distinct metrics with a clear physical meaning (Cardou et al., 2010). Although this is an alternative approach to dexterity analysis, it entails a significant drawback, namely, being applicable only to uniformly actuated manipulators.

Other metrics, not based on the Jacobian, such as *motion/force transmission index* Wang et al. (2010) and *power manipulability* (Mansouri and Ouali, 2011), lie outside the scope of this paper. The former is based on the power coefficient to evaluate the motion/force transmissibility from a wrench to a twist, while the latter concerns the study of power within the mechanism.

## 7.2 Condition-number Minimization

The condition number  $\kappa$  of a matrix  $\mathbf{J}$ , our Jacobian, is defined as (Golub and Van Loan, 2012):

$$\kappa = \|\mathbf{J}\| \|\mathbf{J}^{-1}\| \quad (62)$$

where  $\|\cdot\|$  denotes any norm of its matrix argument. Note that the Frobenius norm is frame-invariant and analytic, i.e., it admits infinitely many derivatives w.r.t. it, gradient methods thus being applicable to minimizing the condition number over architecture parameters and posture variables. Therefore, the Frobenius norm is used throughout this paper. Moreover, we use the homogeneous Jacobian,  $\mathbf{J}_h$ , instead of the raw Jacobian,  $\mathbf{J}$ , to allow for the computation of the condition number  $\kappa$ , and hence,

$$\kappa = \|\mathbf{J}_h\| \|\mathbf{J}_h^{-1}\| \quad (63)$$

where  $\mathbf{J}_h$  is obtained upon normalization of  $\mathbf{J}$  (Angeles, 2014), namely,

$$\mathbf{J}_h = \mathbf{J} \text{diag}\left(\frac{1}{L} \quad \frac{1}{L} \quad 1\right) \quad (64)$$

where  $L$  is the characteristic length, to be determined in the sequel. Of course, this normalization calls for a redefinition of the kinematic variables, Cartesian or joint coordinates, to ensure that the kinematic relations are preserved. It is noteworthy that PKMs usually involve two Jacobians, namely, the forward Jacobian  $\mathbf{K}$  and the inverse Jacobian  $\mathbf{J}_r$ . The inverse Jacobian  $\mathbf{J}_r$  is dimensionally homogeneous because all four actuators are of the same class, namely, prismatic joints. For the purpose of rendering the forward Jacobian matrix  $\mathbf{K}$  dimensionally homogeneous, we redefine it in the form (Angeles, 2014)

$$\mathbf{K} = [\mathbf{K}_p \quad \mathbf{k}_o] \quad (65)$$

where the  $4 \times 2$  matrix  $\mathbf{K}_p$  is the position sub-Jacobian and the four-dimensional vector array  $\mathbf{k}_o$  the orientation sub-Jacobian. Hence, the homogeneous forward Jacobian takes the form

$$\mathbf{K}_h = \left[ \frac{1}{L} \mathbf{K}_p \quad \mathbf{k}_o \right] \quad (66)$$

Thus, the isotropy condition for  $\mathbf{K}_h$  is

$$\mathbf{K}_h^T \mathbf{K}_h = \begin{bmatrix} \frac{1}{L^2} \mathbf{K}_p^T \mathbf{K}_p & \frac{1}{L} \mathbf{K}_p^T \mathbf{k}_o \\ \frac{1}{L} \mathbf{k}_o^T \mathbf{K}_p & \mathbf{k}_o^T \mathbf{k}_o \end{bmatrix} = \sigma^2 \mathbf{1} \quad (67)$$

where  $\sigma > 0$  is a nondimensional scalar and  $\mathbf{1}$  is the  $3 \times 3$  identity matrix. An architecture is considered isotropic as long as its corresponding Jacobian matrix can be rendered isotropic, i.e., with identical singular values, at least at one configuration over the entire workspace (Angeles, 2014). If the isotropy condition does not have a solution, i.e., the manipulator at hand cannot reach a configuration that is isotropic, which is the case at point, then a configuration of minimum condition number is sought.

The condition number of  $\mathbf{K}_h$ , a dimensionally-homogeneous rectangular matrix, based on the Frobenius norm, is computed as

$$\kappa(\mathbf{K}_h) = \frac{1}{3} \sqrt{\text{tr}(\mathbf{K}_h^T \mathbf{K}_h) \text{tr}[(\mathbf{K}_h^T \mathbf{K}_h)^{-1}]} \quad (68)$$

To yield the minimum value of  $\kappa(\mathbf{K}_h)$  and the characteristic length of the optimum architecture, we minimize  $\kappa^2(\mathbf{K}_h)$  instead, to simplify the ensuing calculating. Thus, the problem is now

$$\min_{\mathbf{x}} \kappa^2(\mathbf{K}_h) \quad (69)$$

subject to three geometric constraints:

$$l > 0, l_3 \geq 0, \zeta > 0 \quad (70)$$

the design vector  $\mathbf{x}$  being given by

$$\mathbf{x} = [x_1, x_2, x_3, x_4]^T \equiv [\alpha, \beta, \zeta, L]^T \quad (71)$$

Let

$$z = \kappa^2(\mathbf{K}_h) \equiv \frac{1}{9} \text{tr}(\mathbf{P}) \text{tr}(\mathbf{P}^{-1}), \quad \mathbf{P} \equiv \mathbf{K}_h^T \mathbf{K}_h \quad (72)$$

when  $z$  attains a stationary value, needed for a minimum, its partial derivative with respect to  $\mathbf{x}$  vanishes, i.e.,

$$\frac{\partial z}{\partial \mathbf{x}} = \mathbf{0} \quad (73)$$

The foregoing partial derivative is now calculated. To this end, we recall some key relations (Beyer and Selby, 1984)

$$\begin{aligned} \frac{\partial[\text{tr}(\mathbf{P}) \text{tr}(\mathbf{P}^{-1})]}{\partial x_i} &\equiv \\ \frac{\partial \text{tr}(\mathbf{P})}{\partial x_i} \text{tr}(\mathbf{P}^{-1}) + \text{tr}(\mathbf{P}) \frac{\partial \text{tr}(\mathbf{P}^{-1})}{\partial x_i} &= \frac{\partial \text{tr}(\mathbf{P})}{\partial \mathbf{P}} \frac{\partial \mathbf{P}}{\partial x_i} \text{tr}(\mathbf{P}^{-1}) + \text{tr}(\mathbf{P}) \frac{\partial \text{tr}(\mathbf{P}^{-1})}{\partial \mathbf{P}^{-1}} \frac{\partial \mathbf{P}^{-1}}{\partial x_i} \end{aligned} \quad (74)$$

which, after straightforward manipulations, leads to

$$\frac{\partial \mathbf{P}}{\partial x_i} \text{tr}(\mathbf{P}^{-1}) - \text{tr}(\mathbf{P}) \mathbf{P}^{-1} \frac{\partial \mathbf{P}}{\partial x_i} \mathbf{P}^{-1} = \mathbf{O}, \quad \text{for } i = 1, 2, 3, 4 \quad (75)$$

where  $\mathbf{O}$  is the  $3 \times 3$  zero matrix.

The dimensionally homogeneous matrix  $\mathbf{K}_h$  can be expressed in block form as

$$\mathbf{K}_h = \begin{bmatrix} \mathbf{0} & \mathbf{a} & \mathbf{c} \\ \mathbf{b} & \mathbf{0} & \mathbf{d} \end{bmatrix} \quad (76)$$

where

$$\mathbf{a} = \frac{1}{L} \begin{bmatrix} K_{11} \\ K_{21} \end{bmatrix}, \quad \mathbf{b} = \frac{1}{L} \begin{bmatrix} K_{32} \\ K_{42} \end{bmatrix}, \quad \mathbf{c} = \begin{bmatrix} K_{13} \\ K_{23} \end{bmatrix}, \quad \mathbf{d} = \begin{bmatrix} K_{33} \\ K_{43} \end{bmatrix}, \quad \mathbf{0} = \begin{bmatrix} 0 \\ 0 \end{bmatrix} \quad (77)$$

Therefore,

$$\mathbf{P} \equiv \mathbf{K}_h^T \mathbf{K}_h = \begin{bmatrix} \mathbf{0}^T & \mathbf{b}^T \\ \mathbf{a}^T & \mathbf{0}^T \\ \mathbf{c}^T & \mathbf{d}^T \end{bmatrix} \begin{bmatrix} \mathbf{0} & \mathbf{a} & \mathbf{c} \\ \mathbf{b} & \mathbf{0} & \mathbf{d} \end{bmatrix} = \begin{bmatrix} \|\mathbf{b}\|^2 & 0 & \mathbf{b}^T \mathbf{d} \\ 0 & \|\mathbf{a}\|^2 & \mathbf{a}^T \mathbf{c} \\ \mathbf{d}^T \mathbf{b} & \mathbf{c}^T \mathbf{a} & \|\mathbf{c}\|^2 + \|\mathbf{d}\|^2 \end{bmatrix} \equiv [\mathbf{p}_1 \quad \mathbf{p}_2 \quad \mathbf{p}_3] \quad (78)$$

whose inverse can be readily derived:

$$\begin{aligned} \mathbf{P}^{-1} &\equiv \frac{1}{\Delta} \begin{bmatrix} (\mathbf{p}_2 \times \mathbf{p}_3)^T \\ (\mathbf{p}_3 \times \mathbf{p}_1)^T \\ (\mathbf{p}_1 \times \mathbf{p}_2)^T \end{bmatrix} \\ &= \frac{1}{\Delta} \begin{bmatrix} \|\mathbf{a}\|^2(\|\mathbf{c}\|^2 + \|\mathbf{d}\|^2) - (\mathbf{a}^T \mathbf{c})^2 & (\mathbf{a}^T \mathbf{c})(\mathbf{b}^T \mathbf{d}) & -\|\mathbf{a}\|^2(\mathbf{b}^T \mathbf{d}) \\ (\mathbf{b}^T \mathbf{d})(\mathbf{c}^T \mathbf{a}) & \|\mathbf{b}\|^2(\|\mathbf{c}\|^2 + \|\mathbf{d}\|^2) - (\mathbf{b}^T \mathbf{d})^2 & -\|\mathbf{b}\|^2(\mathbf{a}^T \mathbf{c}) \\ -\|\mathbf{a}\|^2(\mathbf{d}^T \mathbf{b}) & -\|\mathbf{b}\|^2(\mathbf{c}^T \mathbf{a}) & \|\mathbf{a}\|^2\|\mathbf{b}\|^2 \end{bmatrix} \end{aligned} \quad (79)$$

where

$$\Delta \equiv \det(\mathbf{P}) = \mathbf{p}_1 \times \mathbf{p}_2 \cdot \mathbf{p}_3 \equiv \|\mathbf{b}\|^2[\|\mathbf{a}\|^2\|\mathbf{c}\|^2 - (\mathbf{c}^T \mathbf{a})^2] + \|\mathbf{a}\|^2[\|\mathbf{b}\|^2\|\mathbf{d}\|^2 - (\mathbf{b}^T \mathbf{d})^2] \quad (80)$$

Thus,

$$\text{tr}(\mathbf{P}) \equiv \|\mathbf{a}\|^2 + \|\mathbf{b}\|^2 + \|\mathbf{c}\|^2 + \|\mathbf{d}\|^2 \quad (81)$$

$$\begin{aligned} \text{tr}(\mathbf{P}^{-1}) &\equiv \frac{1}{\Delta} [\|\mathbf{a}\|^2(\|\mathbf{b}\|^2 + \|\mathbf{c}\|^2 + \|\mathbf{d}\|^2) + \|\mathbf{b}\|^2(\|\mathbf{c}\|^2 + \|\mathbf{d}\|^2) \\ &\quad - (\mathbf{a}^T \mathbf{c})^2 - (\mathbf{b}^T \mathbf{d})^2] \end{aligned} \quad (82)$$

Substituting Eqs. (78), (79), (81) and (82) into Eq. (75), a system of four equations is obtained. To find the optimum solution, the architecture of the robot is given as  $l = 0.6$  m,  $l_3 = 0.4$  m,  $f_1 = 0.3$  m,  $d = 0.1$  m,  $e = 0$  m and the initial guess of  $\mathbf{x}$ , including both the configuration variables  $\alpha, \beta, \zeta$  and the characteristic length  $L$ , were assigned as

$$\mathbf{x}_{\text{init}} = [0, 0, 0.2, 0.2]^T \quad (83)$$

The Newton-Raphson method was implemented to obtain the optimum. It should be noted that a direct-search method, Nelder-Mead simplex, not relying on gradients, can also be used to solve the foregoing optimization problem with similar results, although it takes a greater number of iterations to converge. In this case, Mathematica reports a time of 0.2031 s and 1.2969 s for Newton-Raphson

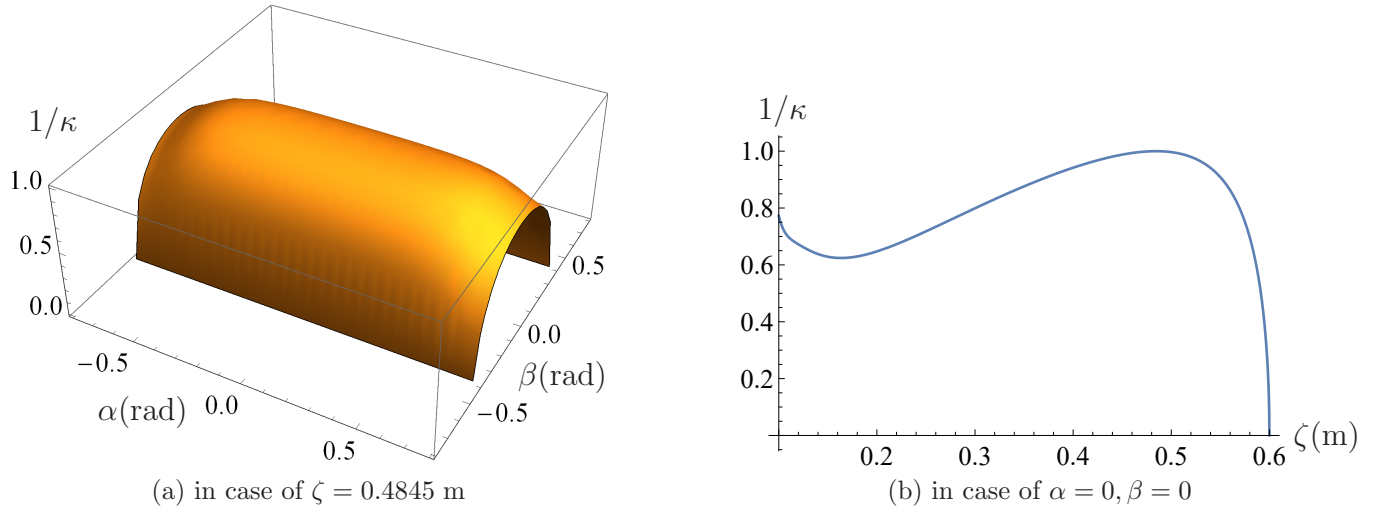


Figure 7: Reciprocal of condition number of Jacobian matrix

method and Nelder-Mead simplex method, respectively. The results thus obtained are displayed below:

$$\mathbf{x}_{\text{opt}} = [0, 0, 0.3, 0.2496]^T \quad (84)$$

whose last component, the characteristic length, is

$$L = 0.2496 \text{ m} \quad (85)$$

Using this number to homogenize the Jacobian of the robot, with the optimum architectural parameters and postural variables, the minimum condition number of interest is obtained as

$$\kappa_{\text{min}} = 1.00013 \approx 1.0 \quad (86)$$

It is noteworthy that the value of  $\zeta$  obtained via the minimization of the condition number of  $\mathbf{K}$  is different from its counterpart when minimizing the condition number of  $\mathbf{J}_h$ , as given in Eq. (64). Thus, the position  $\zeta = 0.3$  m here, should not be taken for granted as the value at the optimum posture.

Moreover, if a tool, with a length  $h$ , is added at the said point  $P$ , the condition number of the resulting Jacobian, mapped from joint-rates to the new tool-head velocity, will change accordingly. Thus the aforementioned method is used to obtain the optimum length of the tool; the result obtained numerically is

$$h = 0.2874 \text{ m} \quad (87)$$



which yields a minimum condition number

$$\kappa_{\min} = 1.0270 \approx 1.0 \quad (88)$$

which is quite close to isotropy. Now, as tools are usually obtained off-the-shelf, the user is not in a position to fix their length. The logical approach here is to modify the MP so as to accommodate the tool in such a way that its protrusion below the bottom of the MP be as close as possible to the optimum found above.

### 7.3 Kinetostatic Conditioning Index: KCI

Hence, with the results of optimum posture based on the minimum condition number, the KCI of the PKM is

$$\text{KCI} = 99.9869\% \quad (89)$$

One can readily conclude that the manipulator is closest to isotropy at a configuration given by  $\zeta = 0.4845$  m,  $\alpha = 0$ ,  $\beta = 0$ . Notice that the value of  $\zeta$  is different from that of Eq. (84).

### 7.4 Global Conditioning Index: GCI

In order to evaluate the GCI, we resort to a numerical method because of the complexity of the expression of the condition number (Gosselin and Angeles, 1991). Moreover, since  $1/\kappa$  approaches zero at points near singularities, sample points near singularities have a reduced impact on the result of the numerical computation of the GCI. Therefore, a simplified numerical approach was introduced to approximately calculate the GCI by a discrete sum (Li and Xu, 2007):

$$\text{GCI} \approx \frac{1}{N} \sum_i^N \frac{1}{\kappa_i} \quad (90)$$

where the workspace has been discretized into a set of  $N$  points,  $\kappa_i$  being the value of  $\kappa$  evaluated at the  $i$ th point. Thus the result obtained numerically is

$$\text{GCI} = 0.7447 \quad (91)$$

## 8 Conclusions

A systematic kinematics-cum-dexterity analysis of a novel three-dof redundantly-actuated PKM was reported. Firstly, the mobility of the mechanism is analyzed by means of Lie-group algebra. Then, closed-form solutions for the inverse-displacement problem are obtained, whereas more

complex direct-displacement relations are derived in the form of a sixth-degree polynomial whose roots at a given set of actuated joint variables call for a numerical method. Moreover, the velocity analysis is conducted before analyzing the four types of singularities. In terms of characteristics of the Jacobian matrix, the condition number as well as the KCI and the GCI, are used to characterize the robot dexterity. We cope with the dimensionally inhomogeneity of the Jacobian matrices by means of the characteristic length using the Newton-Raphson method. It was shown that the KCI of the mechanism is close to its lower bound of unity, while its GCI is close to 75%, or quite acceptable.

## Acknowledgements

The first author would like, first, to acknowledge the China Scholarship Council (CSC) and the Department of Education of Zhejiang Province for their financial support. The work was supported by: the National Science Foundation of China (NSFC) under Grant Nos. 51525504 and U1713202; and Natural Science Foundation of Zhejiang Province under Grant LZ14E050005. The second author acknowledges the support of Natural Sciences and Engineering Research Council of Canada (NSERC) through its Postdoctoral Fellowship Program. The third author acknowledges NSERC's support through Grant No. 4532-2010.

## References

- Jorge Angeles. The qualitative synthesis of parallel manipulators. *ASME Journal of Mechanical Design*, 126(4):617–624, 2004.
- Jorge Angeles. *Fundamentals of Robotic Mechanical Systems Theory, Methods, and Algorithms*. Springer, 2014.
- William H Beyer and Samuel M Selby. *CRC Standard Mathematical Tables*, volume 28. CRC Press Boca Raton, FL, 1984.
- Zhuming M Bi and Yan Jin. Kinematic modeling of Exechon parallel kinematic machine. *Robotics and Computer-Integrated Manufacturing*, 27(1):186–193, 2011.
- Philippe Cardou, Samuel Bouchard, and Clément Gosselin. Kinematic-sensitivity indices for dimensionally nonhomogeneous Jacobian matrices. *IEEE Transactions on Robotics*, 26(1):166–173, 2010.
- Stéphane Caro, Waseem Ahmad Khan, Damiano Pasini, and Jorge Angeles. The rule-based conceptual design of the architecture of serial schönflies-motion generators. *Mechanism and Machine Theory*, 45(2):251–260, 2010.
- Dimitar Chakarov. Study of the antagonistic stiffness of parallel manipulators with actuation redundancy. *Mechanism and Machine Theory*, 39(6):583–601, 2004.

- Chang-Hwan Choi, Hee-Seong Park, Seong-Hyun Kim, Hyo-Jik Lee, Jong-Kwang Lee, Ji-Sub Yoon, and Byung-Seok Park. A manipulator workspace generation algorithm using a singular value decomposition. In *Control, Automation and Systems, 2008. ICCAS 2008. International Conference on*, pages 163–168. IEEE, 2008.
- John J Craig. *Introduction to Robotics: Mechanics and Control*, volume 3. Pearson/Prentice Hall Upper Saddle River, NJ, USA:, 2005.
- Enrique Cuan-Urquizo and Ernesto Rodriguez-Leal. Kinematic analysis of the 3-cup parallel mechanism. *Robotics and Computer-Integrated Manufacturing*, 29(5):382–395, 2013.
- Hussein de la Torre and Ernesto Rodriguez-Leal. Instantaneous kinematics analysis via screw-theory of a novel 3-crc parallel mechanism. *International Journal of Advanced Robotic Systems*, 13(3):128, 2016.
- Tie Fu, Xin Han, Yaya Zhu, and Hongsheng Ding. Type synthesis of 2R1T parallel mechanism based on Lie group theory. *Transactions of Beijing Institute of Technology*, 11:002, 2014.
- Gene H Golub and Charles F Van Loan. *Matrix Computations*, volume 3. JHU Press, 2012.
- Clément Gosselin. The optimum design of robotic manipulators using dexterity indices. *Robotics and Autonomous systems*, 9(4):213–226, 1992.
- Clément Gosselin and Jorge Angeles. Singularity analysis of closed-loop kinematic chains. *IEEE Transactions on Robotics and Automation*, 6(3):281–290, 1990.
- Clément Gosselin and Jorge Angeles. A global performance index for the kinematic optimization of robotic manipulators. *Journal of Mechanical Design*, 113(3):220–226, 1991.
- Clément Gosselin and Louis-Thomas Schreiber. Redundancy in parallel mechanisms: A review. *Applied Mechanics Reviews*, 70(1):010802, 2018.
- Marc Gouttefarde and Clément Gosselin. Wrench-closure workspace of six-dof parallel mechanisms driven by 7 cables. *Transactions of the Canadian Society for Mechanical Engineering*, 29(4): 541–552, 2005.
- Chanhee Han, Jinwook Kim, Jongwon Kim, and Frank Chongwoo Park. Kinematic sensitivity analysis of the 3-upu parallel mechanism. *Mechanism and Machine Theory*, 37(8):787–798, 2002.
- Jacques M Hervé. Analyse structurelle des mécanismes par groupe des déplacements. *Mechanism and Machine Theory*, 13(4):437–450, 1978.
- Jacques M Hervé. The Lie group of rigid body displacements, a fundamental tool for mechanism design. *Mechanism and Machine theory*, 34(5):719–730, 1999.
- Mir Amin Hosseini. Kinematic synthesis of a novel rapid spherical crs/pu parallel manipulator. *Mechanism and Machine Theory*, 93:26–38, 2015.

- Long Huang, Chenhan Guang, Yang Yang, and Peng Su. Type synthesis of parallel 2R1T remote center of motion mechanisms based on screw theory. In *MATEC Web of Conferences*, volume 95, page 08009. EDP Sciences, 2017.
- Sönke Kock and Walter Schumacher. A parallel xy manipulator with actuation redundancy for high-speed and active-stiffness applications. In *Proceedings. 1998 IEEE International Conference on Robotics and Automation*, volume 3, pages 2295–2300. IEEE, 1998.
- Qinchuan Li and Jacques Marie Hervé. Type synthesis of 3-dof rpr-equivalent parallel mechanisms. *IEEE Transactions on Robotics*, 30(6):1333–1343, 2014.
- Qinchuan Li, Zhen Huang, and Jacques Marie Hervé. Type synthesis of 3R2T 5-dof parallel mechanisms using the Lie group of displacements. *IEEE Transactions on Robotics and Automation*, 20(2):173–180, 2004.
- Yangmin Li and Qingsong Xu. Kinematic analysis of a 3-prs parallel manipulator. *Robotics and Computer-Integrated Manufacturing*, 23(4):395–408, 2007.
- Mario Luces, James K Mills, and Beno Benhabib. A review of redundant parallel kinematic mechanisms. *Journal of Intelligent & Robotic Systems*, 86(2):175–198, 2017.
- Imed Mansouri and Mohammed Ouali. The power manipulability—a new homogeneous performance index of robot manipulators. *Robotics and Computer-Integrated Manufacturing*, 27(2):434–449, 2011.
- Jean-Pierre Merlet. Redundant parallel manipulators. *Laboratory Robotics and Automation*, 8(1):17–24, 1996.
- Jean-Pierre Merlet. Jacobian, manipulability, condition number, and accuracy of parallel robots. *Journal of Mechanical Design*, 128(1):199–206, 2006a.
- Jean-Pierre Merlet. *Parallel Robots*, volume 128. Springer Science & Business Media, 2006b.
- Jean-Pierre Merlet, Clément Gosselin, and Tian Huang. Parallel mechanisms. In Bruno Siciliano and Oussama Khatib, editors, *Springer Handbook of Robotics*, chapter 18. Springer, 2016.
- Andreas Müller. On the terminology and geometric aspects of redundant parallel manipulators. *Robotica*, 31(1):137–147, 2013.
- Yanbing Ni, Biao Zhang, Yupeng Sun, and Yuan Zhang. Accuracy analysis and design of A3 parallel spindle head. *Chinese Journal of Mechanical Engineering*, 29(2):239–249, 2016.
- Sarosh Patel and Tarek Sobh. Manipulator performance measures—a comprehensive literature survey. *Journal of Intelligent & Robotic Systems*, 77(3-4):547–570, 2015.
- Francois Pierrot, Vincent Nabat, Olivier Company, Sebastien Krut, and Philippe Poignet. Optimal design of a 4-dof parallel manipulator: From academia to industry. *IEEE Transactions on Robotics*, 25(2):213–224, 2009.

- J Kenneth Salisbury and John J Craig. Articulated hands: Force control and kinematic issues. *The International Journal of Robotics Research*, 1(1):4–17, 1982.
- Bruno Siciliano. The Tricept robot: Inverse kinematics, manipulability analysis and closed-loop direct kinematics algorithm. *Robotica*, 17(4):437–445, 1999.
- Yimin Song, Pengpeng Han, and Panfeng Wang. Type synthesis of 1T2R and 2R1T parallel mechanisms employing conformal geometric algebra. *Mechanism and Machine Theory*, 121:475–486, 2018.
- Lung-Wen Tsai. *Robot Analysis: the Mechanics of Serial and Parallel Manipulators*. John Wiley & Sons, 1999.
- Joachim Wahl. Articulated tool head, 2002. US Patent 6431802.
- Hui Wang, Wen Li, Haitao Liu, Jianxin Zhang, and Songtao Liu. Conceptual design and dimensional synthesis of a novel parallel mechanism for lower-limb rehabilitation. *Robotica*, pages 1–12, 2018.
- Jinsong Wang, Jun Wu, Tiemin Li, and Xinjun Liu. Workspace and singularity analysis of a 3-dof planar parallel manipulator with actuation redundancy. *Robotica*, 27(1):51–57, 2009a.
- Jinsong Wang, Chao Wu, and Xin-Jun Liu. Performance evaluation of parallel manipulators: Motion/force transmissibility and its index. *Mechanism and Machine Theory*, 45(10):1462–1476, 2010.
- Liping Wang, Jun Wu, Jinsong Wang, and Zheng You. An experimental study of a redundantly actuated parallel manipulator for a 5-dof hybrid machine tool. *IEEE/ASME Transactions on Mechatronics*, 14(1):72–81, 2009b.
- Liping Wang, Huayang Xu, and Liwen Guan. Optimal design of a 3-puu parallel mechanism with 2R1T dofs. *Mechanism and Machine Theory*, 114:190–203, 2017.
- Lingmin Xu, Qinchuan Li, Ningbin Zhang, and Qiaohong Chen. Mobility, kinematic analysis, and dimensional optimization of new three-degrees-of-freedom parallel manipulator with actuation redundancy. *Journal of Mechanisms and Robotics*, 9(4):041008, 2017a.
- Lingmin Xu, Qinchuan Li, Junhua Tong, and Qiaohong Chen. Tex3: An 2R1T parallel manipulator with minimum dof of joints and fixed linear actuators. *International Journal of Precision Engineering and Manufacturing*, 19(2):227–238, 2018a.
- Lingmin Xu, Xubiao Zhu, Wei Ye, Qinchuan Li, and Qiaohong Chen. Kinematic analysis and dimensional synthesis of a new 2R1T parallel kinematic machine. In *ASME 2018 International Design Engineering Technical Conferences and Computers and Information in Engineering Conference*, pages V05AT07A030–V05AT07A030. American Society of Mechanical Engineers, 2018b.

- Yundou Xu, Dongsheng Zhang, Jiantao Yao, and Yongsheng Zhao. Type synthesis of the 2R1T parallel mechanism with two continuous rotational axes and study on the principle of its motion decoupling. *Mechanism and Machine Theory*, 108:27–40, 2017b.
- Abdullah Yaşır and Gökhan Kiper. Structural synthesis of 2R1T type mechanisms for minimally invasive surgery applications. In *International Workshop on Computational Kinematics*, pages 31–38. Springer, 2017.
- Tsuneo Yoshikawa. Manipulability of robotic mechanisms. *The International Journal of Robotics Research*, 4(2):3–9, 1985.
- Dimiter Zlatanov, Ilian A Bonev, and Clément Gosselin. Constraint singularities of parallel mechanisms. In *Robotics and Automation, 2002. Proceedings. ICRA '02. IEEE International Conference on*, volume 1, pages 496–502. IEEE, 2002.
- Matteo Zoppi, Dimiter Zlatanov, and Rezia Molfino. Kinematics analysis of the Exechon tripod. In *ASME 2010 international design engineering technical conferences and computers and information in engineering conference*, pages 1381–1388. American Society of Mechanical Engineers, 2010.